Materials Science in Semiconductor Processing 56 (2016) 59–65

Contents lists available at ScienceDirect

Materials Science in Semiconductor Processing

journal homepage: www.elsevier.com/locate/mssp

# Photoluminescence from *c*-axis oriented ZnO films synthesized by sol-gel with diethanolamine as chelating agent

Oscar Marin [a,b,*], Mónica Tirado [a,c,d], Nicolás Budini [e], Edgar Mosquera [b], Carlos Figueroa [f], David Comedi [a,c,f,*]

[a] NanoProject, Facultad de Ciencias Exactas y Tecnología, Universidad Nacional de Tucumán, Avenida Independencia 1800, San Miguel de Tucumán, 4000 Argentina
[b] Laboratorio de Materiales Funcionales a Nanoescala, Departamento de Ciencias de los Materiales, Facultad de Ciencias Físicas y Matemáticas, Universidad de Chile, Beauchef 851, Santiago, Chile
[c] Consejo Nacional de Investigaciones Científicas y Técnicas (CONICET), Argentina
[d] Laboratorio de Nanomateriales y Propiedades Dieléctricas (LNPD), Facultad de Ciencias Exactas y Tecnología, Universidad Nacional de Tucumán, Avenida Independencia 1800, San Miguel de Tucumán, 4000 Argentina
[e] Instituto de Física del Litoral, UNL, CONICET, FIQ, Güemes 3450, Santa Fe, S3000GLN Argentina
[f] Laboratorio de Física del Sólido (LAFISO), Departamento de Física, Facultad de Ciencias Exactas y Tecnología, Universidad Nacional de Tucumán, Argentina

ARTICLE INFO

*Article history:*
Received 26 May 2016
Received in revised form
11 July 2016
Accepted 13 July 2016

*Keywords:*
ZnO films
Sol-gel technique
Diethanolamine
Thermal annealing
Photoluminescence

ABSTRACT

ZnO films were synthesized on $SiO_2$/Si substrates through the sol-gel technique using diethanolamine as chelating agent and annealed in $Ar+O_2$ atmospheres with different $O_2$ flow-rates in the 10–100 sccm range. Samples were studied by scanning electron microscopy and X-ray diffraction, evidencing a nanostructured morphology with a preferential orientation along the (0 0 2) direction (*c*-axis orientation), which is uncommon when diethanolamine is used as the chelating agent. The room temperature photoluminescence spectra show strong UV emissions at around 375 and 384 nm from near band-edge transitions and phonon replica, and a broad defect-related band extending from the visible to near infrared (~500–800 nm). The analysis of the defect-related emission band and its various components as a function of the $O_2$ flow-rate is discussed in terms of contributions from specific luminescent point defect centers established during annealing.



## 1. Introduction

Zinc oxide is considered an important and promising material. Reasons for this include low-cost, simple and controllable synthesis processes of a wide diversity of nanostructures, such as nanocones [1], nanoparticles [2], nanowires [3], nanostructured films [4]. Furthermore, ZnO is a II–VI semiconductor with interesting optoelectronic properties due to its wide band gap of 3.37 eV and large excitonic binding energy of 60 meV, which is larger than the mean thermal energy at room temperature (RT) [1]. Hence ZnO finds many applications in diverse optoelectronic devices, particularly in light-emitting diodes [5]. Other interesting applications have been proposed for ZnO in catalysis [6], sensors [7], optical waveguides [8] and photodetectors [9].

Nanostructured ZnO can be synthesized through different processes, like vapor transport with and without metallic catalyst [1,3], sol-gel [10,11], pulsed laser deposition [12], electrophoretic deposition [2], hydrothermal synthesis [13] and molecular beam epitaxy [14], among others. The sol-gel synthesis is a powerful and interesting route, as it involves processes at intermediate temperatures with low costs and easy implementation [11]. This technique involves transformations of a molecular precursor onto a stable condensed oxide network through several stages, including hydrolysis and polymerization for the formation of the sol precursor and condensation by dehydration, nucleation and growth (commonly achieved through annealing) [11]. When organometallic salts are used as molecular precursors the solvent used is organic [15]. The aminoalcohols – diethanolamine (DEA) and monoethanolamine (MEA) – are the most common chelating agents when zinc acetate is used as a $Zn^{+2}$ source. The reason for this is that these compounds increase the solubility of organometallic zinc salts, improving stability and homogeneity of sol precursors [4,16,17].

The photoluminescence (PL) of nanostructured ZnO has been studied extensively. Regarding ZnO layers synthesized through the sol-gel technique, most studies have focused mainly on the effects

* Corresponding authors at: NanoProject, Facultad de Ciencias Exactas y Tecnología, Universidad Nacional de Tucumán, Avenida Independencia 1800, 4000 San Miguel de Tucumán, Argentina.
*E-mail addresses:* alquimarin@gmail.com (O. Marin), dcomedi@herrera.unt.edu.ar (D. Comedi).

http://dx.doi.org/10.1016/j.mssp.2016.07.007
1369-8001/

of chelating agent/$Zn^{+2}$ ratio [4], pH [17] and annealing temperature [18] on the PL spectrum. However, the effect of oxygen ($O_2$) flow-rate during annealing/growth processes on the PL of sol-gel synthesized ZnO films has been rarely reported.

In this work, ZnO films were synthesized through the sol-gel technique in combination with the spin-coating deposition method. ZnO samples were deposited on silicon (Si) substrates stored in atmospheric air (therefore, naturally oxidized [19]). The influence of $O_2$ flow-rate during the annealing process on the PL at room temperature, and also on morphological and structural properties of the ZnO films, was studied. These results contribute to the understanding of the room-temperature PL spectra from ZnO films grown by the sol-gel technique and the role of point defects controlled by annealing in different $Ar+O_2$ atmospheres. Furthermore, they show that it is possible to obtain highly oriented sol-gel synthesized ZnO layers on oxidized Si substrates, using DEA as chelating agent.

## 2. Experimental details

### 2.1. ZnO fabrication

To prepare the sol precursor, 2.3 g of zinc acetate dihydrate [Aldrich, $Zn(C_2H_3O_2)_2 \cdot 2H_2O$] was diluted in 30 ml of ethanol at 65 °C to obtain a 0.3 M solution. A volume of 1 ml of DEA (Aldrich, $C_4H_{11}NO_2$) was added to obtain a sol with a 1:1 M ratio of $Zn^{+2}$/DEA under constant stirring, until the solution went from white to transparent. After stirring at 65 °C during about 2 h the sol precursor was cooled down to RT. The sol was then aged for 24 h and no precipitates were observed.

ZnO layers were deposited onto *p*-type ⟨1 0 0⟩-oriented Si substrates, which were ultrasonically washed first in acetone, then in ethanol and finally air dried to remove organic contaminants. Substrates were not etching with hydrofluoric acid (HF-etched) prior to deposition, so as to leave a passivating thin layer ( ≈ 2 nm-thick) of native amorphous Si oxide ($SiO_2$) [19,20].

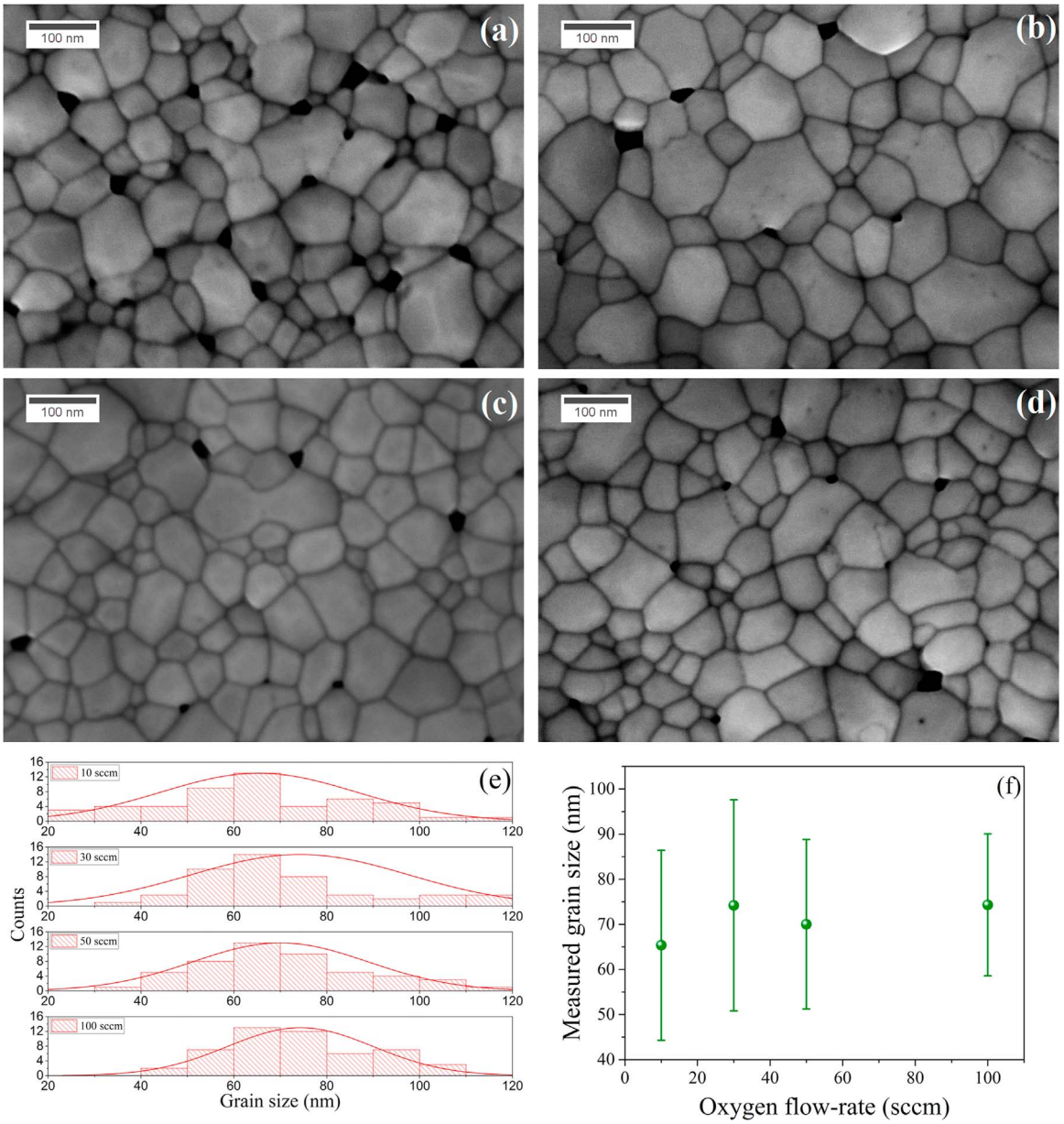


**Fig. 1.** SEM images of the ZnO films annealed under $O_2$ flow-rates of (a) 10 sccm, (b) 30 sccm, (c) 50 sccm and (d) 100 sccm, respectively; (e) grain size distributions obtained from SEM images ($n$=50); (f) measured grain sizes from SEM micrographs.

The sol was deposited by 14 spin-coating/drying cycles (spin-coating: 150 μl of sol at 2000 rpm for 30 s) and dried in an oven at 150 °C for 10 min. After deposition, the samples were kept in a horizontal split tube furnace at 600 °C for 1 h under a flow of argon+oxygen ($Ar+O_2$) gas mixture. The Ar (99.999% purity) flow-rate was fixed at 125 sccm for all experiments, while different $O_2$ (99.999% purity) flow-rates were used, namely 10, 30, 50 and 100 sccm. After 1 h of annealing, the split furnace was opened to quench the sample temperature at RT while maintaining the gas flow to avoid contamination.

### 2.2. Characterization

Samples were studied by X-ray diffraction (XRD), scanning electron microscopy (SEM) and RT PL measurements. XRD patterns were obtained in a Shimadzu XD-D1 diffractometer, operating with the $CuK_\alpha$ line ($\lambda=0.1541$ nm). PL spectra were recorded using a backscattering geometry with a 15 mW He-Cd laser set at a wavelength of 325 nm as the excitation source. The light emitted by the sample was focalized on a CCD spectrometer with two bi-convex lenses. A filter was placed at the entrance of the spectrometer to eliminate scattered laser radiation. The surface morphology of the samples was characterized with SEM.

## 3. Results and discussion

Fig. 1 shows the SEM images obtained for the ZnO samples annealed under different $O_2$ flow-rates. The films evidenced a granular morphology with broad dispersion of grain sizes in the range between 20–120 nm, as observed in the histograms shown in Fig. 1(e). However, by comparing the distribution of grain sizes, no significant differences were observed between the deposited films, as shown in Fig. 1(f).

Fig. 2(a) shows the XRD patterns obtained from the deposited ZnO films. The average crystallite size was obtained from the these patterns by means of the well-known Scherrer's equation, which reads

$$D = \frac{K\lambda}{\beta \cos\theta}, \quad (1)$$

where $D$ is the average crystallite size, $K$ ($\approx 0.9$) is the shape factor, $\beta$ is the FWHM of the diffraction peak in radians, $\theta$ is the Bragg angle and $\lambda$ is the wavelength of the incident X-rays ($CuK\alpha=0.154$ nm). As seen in Fig. 3, a slight variation of crystallite size was observed in the range between 32 and 37 nm around an average value of 34 nm. Together with grain size estimation from SEM images, this allowed us confirming the nanostructured morphology of the films. Analogously to the determination of grain sizes from SEM images, this variation does not represent a significant difference to be considered as being correlated to $O_2$ flow-rate. The difference between the values obtained from Scherrer's equation and from SEM images is due to the fact that only the crystalline fraction of the grains observed in SEM images contributes to the XRD peak intensity.

The XRD patterns evidence a preferential growth orientation of the films along the (0 0 2) direction, corresponding to the $c$-axis of the wurtzite structure. It is worth noting here that such preferential orientation is common for ZnO films [21] and is related to the metastability of the polar $c$-axis, which implies a larger growth rate along the $c$ direction as compared to other crystallographic directions. However, for ZnO films obtained from sol-gel precursors this preferred orientation is generally observed when MEA is used as chelating agent [10,11]. Instead, no strong preferred orientations are usually observed when DEA is used as chelating agent [16]. Indeed, reports on growth of preferentially oriented ZnO films using DEA are seldom found in the literature [22–24].

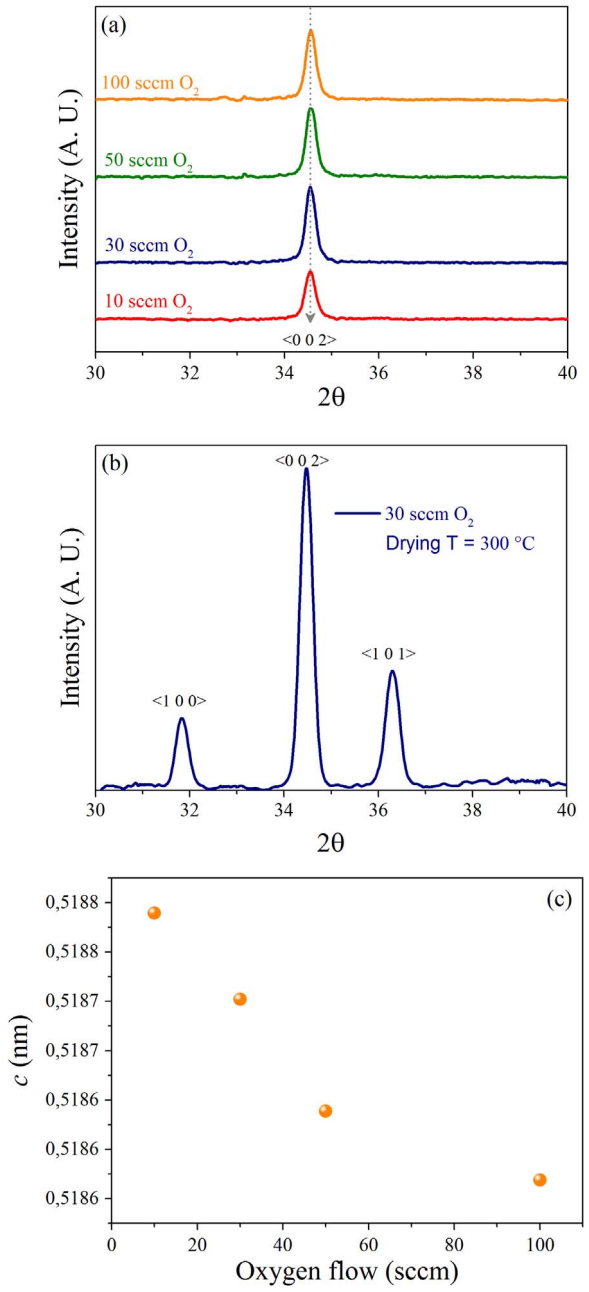


**Fig. 2.** (a) XRD patterns of all samples after drying at 100 °C and annealing; (b) XRD pattern for a test sample dried at 300 °C; (c) variation of the $c$ parameter with $O_2$ flow-rate during annealing.

A key parameter to define the preferential direction of growth is the temperature used during the drying process (previous to annealing); for films synthesized using MEA it has been observed that the (0 0 2) orientation appears at high drying temperatures ($\geq 300$ °C) [25]. In counterpart, when DEA is used, there are reports about the synthesis of ZnO films oriented in the (0 0 2) direction at low drying temperatures, as in our case [24]. In order to prove the influence of this parameter in the preferential orientation of ZnO films, we synthesized a test sample using a drying temperature of 300 °C instead of 150 °C and 30 sccm of $O_2$ (without changing the other parameters). As observed in Fig. 2(b), the peaks corresponding to (1 0 0) and (1 0 1) directions are clearly present, evidencing an opposite behavior to that reported in the

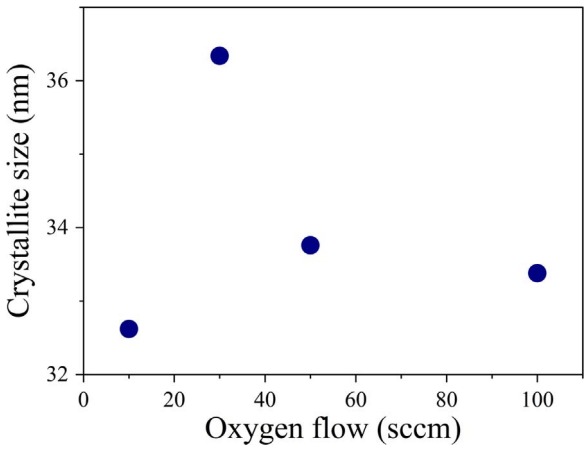


**Fig. 3.** Crystallite sizes obtained by means of Scherrer's equation using the XRD data shown in Fig. 2(a).

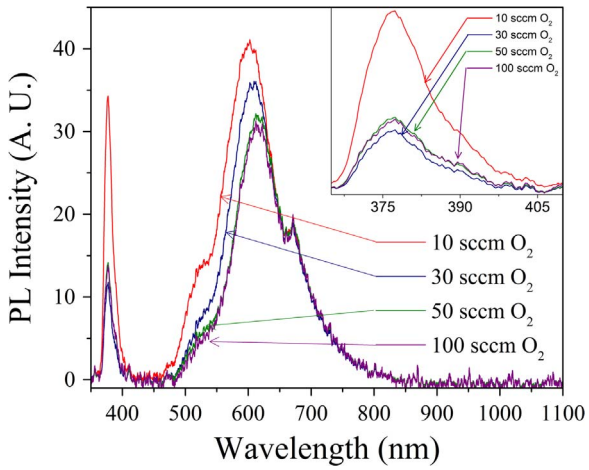


**Fig. 4.** Room temperature photoluminescence spectra obtained from ZnO films annealed under different $O_2$ flow-rates. The inset shows a detail of the emission band in the UV region.

literature regarding the relation between drying temperature and preferential orientation in ZnO films grown using MEA. The origin of this difference between the use of DEA and MEA resides probably on the complexation mechanisms between $Zn^{+2}$ and each aminoalcohol to form the corresponding organometallic complex.

The substrate is another key parameter that could affect the crystallographic properties of the ZnO films [11]. It has been reported that when sol-gel deposition is performed onto amorphous and crystalline substrates it is possible to obtain ZnO films with a preferential orientation along the c-axis. [11,24]. In the case of sol-gel deposition, the orientation is defined during the nucleation stage, at which the preferred *c*-direction orientation of crystallites is defined by energy minimization favoring their growth from the substrate upwards along the c-axis [11]. Hence, the crystalline disorder or amorphousness of the substrate will not necessarily inhibit the preferred orientation of the ZnO film. Taking this into account, and given that native oxide in the silicon substrate has an amorphous nature, a *c*-axis orientation of ZnO films can be expected. However, as mentioned above, it is not usually observed when DEA is used as chelating agent. In our work, the degree of preferential orientation depended mainly on the drying temperature while the $Si/SiO_2$ substrate was the same for all samples. Therefore, according to our results, the variation of $O_2$ flow-rate does not have any sizable effect on the preferential orientation of ZnO films. Since the substrate was the same for all samples, we are left with the fact that the drying temperature was the most important factor affecting the preferential crystalline orientation of our ZnO films. This is expected because crystal nucleation processes at such relatively low temperatures should be limited by kinetic barriers and therefore their rates should be strong functions of the temperature. However, given the complexity of the crystallite formation processes, further experiments should be conducted for a better understanding of this effect and the opposite correlation with the temperature with respect to that observed when MEA is used as chelating agent.

The lattice parameter *c* can be calculated from the (0 0 2) diffraction peak by combining Bragg's law and the equation for spacing between planes

$$\frac{4\sin^2\theta}{n^2\lambda^2} = \frac{4}{3}\left(\frac{h^2+hk+k^2}{a^2}\right) + \frac{l^2}{c^2} \tag{2}$$

where *a* and *c* are the lattice parameters for hexagonal wurtzite, *n* is the diffraction order from Bragg's law and (*h k l*) are the Miller indices of the corresponding family of planes. For the first Bragg reflection ($n=1$), one gets

$$\sin^2\theta = \frac{\lambda^2}{4a^2}\left[\frac{4}{3}\left(h^2+hk+k^2\right) + \frac{l^2}{(c/a)^2}\right]. \tag{3}$$

By substituting (*h k l*) values and $\theta$ for the (0 0 2) diffraction peak in Eq. (3) the *c* parameter is found to be given by the expression

$$c = \frac{\lambda}{\sin\theta}. \tag{4}$$

In this way, the *c* values obtained for the samples annealed under the lowest and highest $O_2$ flow-rates, respectively 10 and 100 sccm, were 0.5188 and 0.5185 nm. A slight but noticeable variation of this parameter as a function of $O_2$ flow-rate during annealing was observed, as shown in Fig. 2(c). Moreover, all the obtained *c* values were lower than the standard value of 0.5207 nm reported for ZnO (JCPDS Card No. 05-0644). The diminution of the *c* parameter has already been observed for samples grown in an $O_2$-rich atmosphere [26].

Fig. 4 shows the measured PL spectra at RT for all samples. A broad emission peak was observed in the visible region, which extends into the near infrared (500–800 nm). There was also a strong ultraviolet (UV) emission band with two components at about 375 and 384 nm, as shown in the inset of Fig. 4 and, in more detail, in Fig. 5(a) and (b). For all samples and over the entire emission range, except for the red component, the PL intensity decreased with increasing $O_2$ flow-rate. In contrast to morphological and structural characteristics, the PL was expected to be strongly affected by small changes in the density of defects which, in general, have an important impact on recombination rates across the bandgap in semiconductors.

Although the PL of ZnO has been widely studied, the origin of emission bands in the visible range remains controversial. Two clear examples of this are the discussions on the origin of the green and yellow components. The green emission has been associated with zinc [14] and oxygen [27] vacancies ($V_{Zn}$ and $V_O$, respectively), while the yellow emission has been attributed to oxygen vacancies and interstitial oxygen ($O_i$) [28]. As for the UV emission at RT, the origin is related to near-edge transitions, involving free and neutral donor bound excitons (FX and $D^0X$) [29], donor-acceptor pairs (DAP) [29,30], acceptor-bound excitons ($A^0X$) [30] and their various order longitudinal-optical (LO) phonon replicas [7].

As mentioned above, and as shown in Fig. 5, the UV emission band can be decomposed in two components located around 375

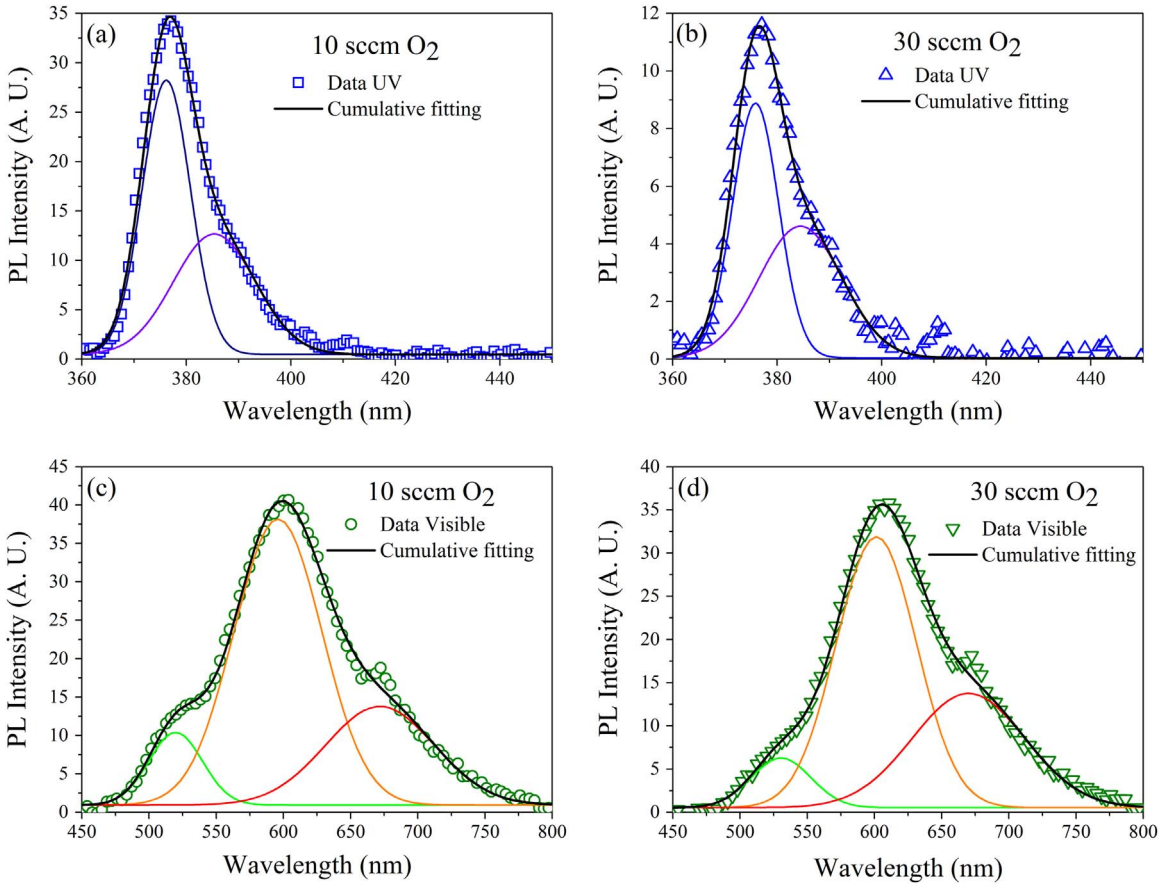


**Fig. 5.** Gaussian function fits of PL spectra from samples annealed under an $O_2$ flow-rate of 10 sccm in the (a) UV and (c) visible regions, and of 30 sccm in the (b) UV and (d) visible regions. (For interpretation of the references to color in this figure legend, the reader is referred to the web version of this article.)

and 384 nm (photon energies of 3.23 and 3.31 eV, respectively). It is interesting to note that these values do not change significantly with the $O_2$ flow-rate during annealing. Furthermore, they agree well with those attributed to the FX and its various order phonon replica contributions, which are broad at RT and hence merge together into the main observed band [27].

To analyze the visible PL components as a function of the $O_2$ flow-rate we considered the following equations, which describe the evolution of point defect concentrations in ZnO during its calcination in an $O_2$-rich ambient [14]:

$$[V_{Zn}]\alpha P_{O_2}^{1/2}; \quad [V_O]\alpha P_{O_2}^{-1/2}; \quad [Zn_i]\alpha P_{O_2}^{-1/2}; \quad [O_i]\alpha P_{O_2}^{1/2}, \tag{5}$$

where $Zn_i$ is interstitial zinc.

As noted, during annealing in $O_2$ excess conditions, both $[V_{Zn}]$ and $[O_i]$ increase with increasing $O_2$ partial pressure ($P_{O2}$), while $[V_O]$ and $[Zn_i]$ decrease. As mentioned above, the yellow emission has been associated in the literature with both $V_O$ and $O_i$. Taking into account the relations given in Eq. (5), $[V_O]$ is expected to decrease and $[O_i]$ to increase with increasing $O_2$ flow-rate. However, the yellow emission in the deposited ZnO samples decreased with increasing $O_2$ flow-rate [see Fig. 6(a)]. Therefore, it is not reasonable to attribute this emission to $[O_i]$ but to $[V_O]$ instead. Similar results have been reported previously, relating yellow emission in ZnO with transitions between electrons in the conduction band to doubly ionized oxygen vacancies ($V_O^{++}$) [1,31].

Based on Eq. (5), $[V_{Zn}]$ increases while $[V_O]$ decreases with the $O_2$ flow-rate during annealing. As shown in Fig. 6(a), the green

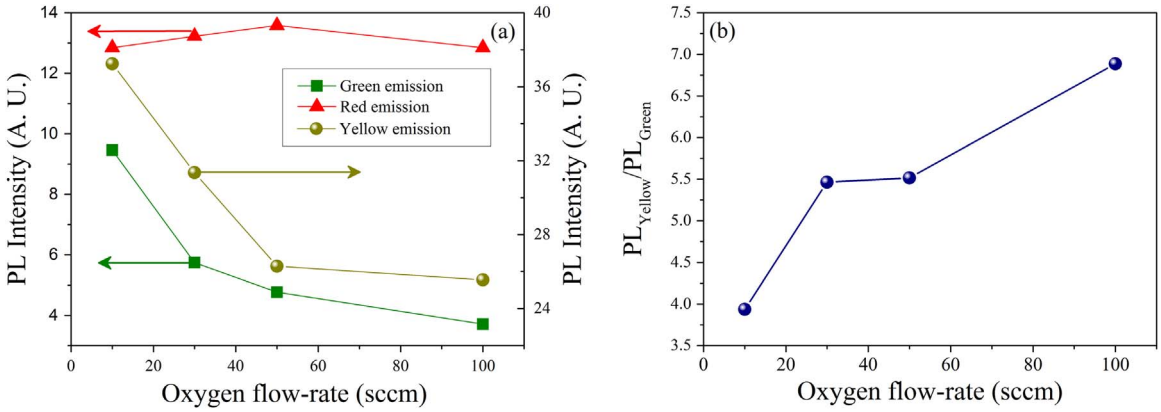


**Fig. 6.** (a) Intensities of green, yellow and red PL components, and (b) $PL_{Yellow}/PL_{Green}$ ratio, as functions of the $O_2$ flow-rate.

emission intensity decreased with increasing $O_2$ flow-rate, which indicates that this component, just like the yellow emission, should be associated with $V_O$. Fig. 6(b) shows the $PL_{Yellow}/PL_{green}$ ratio as a function of the $O_2$ flow-rate. As observed, the intensity of the green emission decreased more rapidly than the yellow emission intensity with increasing $O_2$ flow-rate. This behavior, in turn, suggests that these two emission components are not due to transitions involving the same defect ($V_O$) since, in such case, the ratio $PL_{Yellow}/PL_{green}$ would be nearly constant. An alternative explanation for the origin of the green luminescence involves transitions between $V_O$-$Zn_i$ complex states to the valence band [32–34]. This is in accordance with the obtained experimental results, since both $V_O$ and $Zn_i$ concentrations decreased with increasing $O_2$ flow-rate. This would also explain the different reduction rates of the green and yellow emission intensities with increasing $O_2$ flow-rate.

The red emission has also been related with $Zn_i$, $V_O$ and $O_i$ [28,35,36]. Taking into account the previous discussion about the evolution of point defect concentrations as a function of $O_2$ flow-rate, there is no evidence regarding the role of these in the red emission since, as shown in Fig. 6(a), this component did not change much with increasing $O_2$ flow-rate. An alternative explanation relates the red emission with lattice disorder [37,38]. However, further experiments are needed for a better understanding of the origin of this component.

## 4. Conclusion

ZnO films have been synthesized on $SiO_2$/Si substrates by the sol-gel technique using DEA as the chelating agent and annealed in $Ar+O_2$ atmosphere with fixed Ar and varying $O_2$ flow-rates. A preferential orientation along the *c*-axis direction of wurtzite was observed in all samples. *The drying temperature is the most important factor affecting the degree of preferential orientation in the films.* Under UV excitation, the samples showed an intense UV emission band comprising two components, centered around 375 and 384 nm, and a broad visible emission band which can be decomposed into three (green, yellow and red) components. The UV emission was attributed to the FX and phonon replica contributions, which are broad at RT and hence merge together into the main observed band. From the analysis of the intensity of the different PL components as functions of $O_2$ flow-rate during annealing, the green emission was attributed to transitions from $V_O$-$Zn_i$ complex states to the valence band. The yellow emission, in turn, was attributed to transitions between electrons in the conduction band and doubly ionized oxygen vacancies ($V_O^{++}$). Further experiments should be conducted for a better understanding of the red emission and crystallization mechanisms.

## Acknowledgements

This work was supported by PIUNT 26/E535, CONICET (PID 0414) (Argentina) and FONDECYT No. 3160043 (Chile).

## References

[1] O. Marin, G. Grinblat, A.M. Gennaro, M. Tirado, R.R. Koropecki, D. Comedi, On the origin of white photoluminescence from ZnO nanocones/porous silicon heterostructures at room temperature, Superlattices Microstruct. 79 (2015) 29–37, http://dx.doi.org/10.1016/j.spmi.2014.12.016.
[2] C. Sandoval, O. Marin, S. Real, D. Comedi, M. Tirado, Electrophoretic deposition of ZnO nanostructures: Au nanoclusters on Si substrates induce self-assembled nanowire growth, Mater. Sci. Eng. B: Solid-State Mater. Adv. Technol. 187 (2014) 21–25, http://dx.doi.org/10.1016/j.mseb.2014.04.002.
[3] G. Grinblat, F. Bern, J. Barzola-Quiquia, M. Tirado, D. Comedi, P. Esquinazi, Luminescence and electrical properties of single ZnO/MgO core/shell nanowires, Appl. Phys. Lett. 104 (2014) 0–4, http://dx.doi.org/10.1063/1.4868648.
[4] F. Boudjouan, A. Chelouche, T. Touam, D. Djouadi, S. Khodja, M. Tazerout, Y. Ouerdane, Z. Hadjoub, Effects of stabilizer ratio on photoluminescence properties of sol–gel ZnO nano-structured thin films, J. Lumin. 158 (2015) 32–37, http://dx.doi.org/10.1016/j.jlumin.2014.09.026.
[5] M.T. Chen, M.P. Lu, Y.J. Wu, J. Song, C.Y. Lee, M.Y. Lu, Y.C. Chang, L.J. Chou, Z. L. Wang, L.J. Chen, Near UV LEDs made with in situ doped p-n homojunction ZnO nanowire arrays, Nano Lett. 10 (2010) 4387–4393, http://dx.doi.org/10.1021/nl101907h.
[6] B.V. Kumar, H.S.B. Naik, D. Girija, B.V. Kumar, ZnO nanoparticle as catalyst for efficient green one-pot synthesis of coumarins through Knoevenagel condensation, J. Chem. Sci. 123 (2011) 615–621, http://dx.doi.org/10.1007/s12039-011-0133-0.
[7] R. Viter, V. Khranovskyy, N. Starodub, Y. Ogorodniichuk, S. Gevelyuk, Z. Gertnere, N. Poletaev, R. Yakimova, D. Erts, V. Smyntyna, A. Ubelis, Application of room temperature photoluminescence from ZnO nanorods for salmonella detection, IEEE Sens. J. 14 (2014) 2028–2034, http://dx.doi.org/10.1109/JSEN.2014.2309277.
[8] Z. Jiwei, Z. Liangying, Y. Xi, The dielectric properties and optical propagation loss of c-axis oriented ZnO thin films deposited by sol–gel process, Ceram. Int. 26 (2000) 883–885, http://dx.doi.org/10.1016/S0272-8842(00)00031-6.
[9] S.P. Chang, K.J. Chen, Zinc oxide nanoparticle photodetector, J. Nanomater. 2012 (2012) 1–5, http://dx.doi.org/10.1155/2012/602398.
[10] P. Hosseini Vajargah, H. Abdizadeh, R. Ebrahimifard, M.R. Golobostanfard, Sol–gel derived ZnO thin films: effect of amino-additives, Appl. Surf. Sci. 285 (2013) 732–743, http://dx.doi.org/10.1016/j.apsusc.2013.08.118.
[11] L. Znaidi, Sol-gel-deposited ZnO thin films: a review, Mater. Sci. Eng. B: Solid-State Mater. Adv. Technol. 174 (2010) 18–30, http://dx.doi.org/10.1016/j.mseb.2010.07.001.
[12] M. Benetti, D. Cannatá, F. Di Pietrantonio, E. Verona, P. Verardi, N. Scarisoreanu, D. Matei, G. Dinescu, a Moldovan, M. Dinescu, Structural and piezoelectric properties of pulsed laser deposited ZnO thin films, Superlattices Microstruct. 39 (2006) 366–375, http://dx.doi.org/10.1016/j.spmi.2005.08.073.
[13] Z. Ibupoto, K. Khun, M. Eriksson, M. AlSalhi, M. Atif, A. Ansari, M. Willander, Hydrothermal growth of vertically aligned ZnO nanorods using a biocomposite seed layer of ZnO nanoparticles, Materials 6 (2013) 3584–3597, http://dx.doi.org/10.3390/ma6083584.
[14] Y.W. Heo, D.P. Norton, S.J. Pearton, Origin of green luminescence in ZnO thin film grown by molecular-beam epitaxy, J. Appl. Phys. (2005), http://dx.doi.org/10.1063/1.2064308.
[15] J. Livage, D. Ganguli, Sol-gel electrochromic coatings and devices: a review, Sol. Energy Mater. Sol. Cells 68 (2001) 365–381, http://dx.doi.org/10.1016/S0927-0248(00)00369-X.
[16] S.H. Yoon, D. Liu, D. Shen, M. Park, D.J. Kim, Effect of chelating agents on the preferred orientation of ZnO films by sol–gel process, J. Mater. Sci. 43 (2008) 6177–6181, http://dx.doi.org/10.1007/s10853-008-2929-y.
[17] P. Sagar, P.K. Shishodia, R.M. Mehra, Influence of pH value on the quality of sol–gel derived ZnO films, Appl. Surf. Sci. 253 (2007) 5419–5424, http://dx.doi.org/10.1016/j.apsusc.2006.12.026.
[18] P. Sagar, P.K. Shishodia, R.M. Mehra, H. Okada, A. Wakahara, A. Yoshida, Photoluminescence and absorption in sol-gel-derived ZnO films, J. Lumin. 126 (2007) 800–806, http://dx.doi.org/10.1016/j.jlumin.2006.12.003.
[19] A.H. Al-Bayati, K.G. Orrman-Rossiter, J.A. van den Berg, D.G. Armour, Composition and structure of the native Si oxide by high depth resolution medium energy ion scattering, Surf. Sci. 241 (1991) 91–102, http://dx.doi.org/10.1016/0039–6028(91)90214-D.
[20] T. Miura, M. Niwano, D. Shoji, N. Miyamoto, Kinetics of oxidation on hydrogen-terminated Si(100) and (111) surfaces stored in air, J. Appl. Phys. 79 (1996) 4373, http://dx.doi.org/10.1063/1.362670.
[21] F.A. Garcés, N. Budini, R.D. Arce, J.A. Schmidt, Effect of thickness on structural and electrical properties of Al-doped ZnO films, Thin Solid Films 574 (2015) 162–168, http://dx.doi.org/10.1016/j.tsf.2014.12.013.
[22] R. Ghosh, S. Fujihara, D. Basak, Studies of the optoelectronic properties of ZnO thin films, J. Electron. Mater. 35 (2006) 1728–1733, http://dx.doi.org/10.1007/s11664-006-0226-6.
[23] R. Ghosh, D. Basak, S. Fujihara, Effect of substrate-induced strain on the structural, electrical, and optical properties of polycrystalline ZnO thin films, J. Appl. Phys. 96 (2004) 2689–2692, http://dx.doi.org/10.1063/1.1769598.
[24] S. Chakrabarti, D. Ganguli, S. Chaudhuri, Substrate dependence of preferred orientation in sol–gel-derived zinc oxide films, Mater. Lett. 58 (2004) 3952–3957, http://dx.doi.org/10.1016/j.matlet.2004.09.002.
[25] J.H. Lee, K.H. Ko, B.O. Park, Electrical and optical properties of ZnO transparent conducting films by the sol–gel method, J. Cryst. Growth 247 (2003) 119–125, http://dx.doi.org/10.1016/S0022-0248(02)01907-3.
[26] J.H. Jo, T. Hur, J.S. Kwak, D.Y. Kwon, Y. Hwang, H.K. Kim, Effects of oxygen pressure on the crystalline of ZnO films grown on sapphire by PLD method, J. Korean Phys. Soc. 47 (2005) 300–303.
[27] P.P. Murmu, R.J. Mendelsberg, J. Kennedy, D.A. Carder, B.J. Ruck, A. Markwitz, R. J. Reeves, P. Malar, T. Osipowicz, Structural and photoluminescence properties of Gd implanted ZnO single crystals, J. Appl. Phys. 110 (2011) 033534, http://dx.doi.org/10.1063/1.3619852.
[28] M. Willander, O. Nur, J.R. Sadaf, M.I. Qadir, S. Zaman, A. Zainelabdin, N. Bano, I. Hussain, Luminescence from zinc oxide nanostructures and polymers and their hybrid devices, Materials 3 (2010) 2643–2667, http://dx.doi.org/10.3390/

ma3042643.
[29] A. Teke, Ü. Özgür, S. Doğan, X. Gu, H. Morkoç, B. Nemeth, J. Nause, H.O. Everitt, Excitonic fine structure and recombination dynamics in single-crystalline ZnO, Phys. Rev. B 70 (2004) 195207, http://dx.doi.org/10.1103/PhysRevB.70.195207.
[30] V.A. Fonoberov, K.A. Alim, A.A. Balandin, F. Xiu, J. Liu, Photoluminescence investigation of the carrier recombination processes in ZnO quantum dots and nanocrystals, Phys. Rev. B 73 (2006) 165317, http://dx.doi.org/10.1103/PhysRevB.73.165317.
[31] Z.M. Liao, H.Z. Zhang, Y.B. Zhou, J. Xu, J.M. Zhang, D.P. Yu, Surface effects on photoluminescence of single ZnO nanowires, Phys. Lett. Sect. A: Gen. At. Solid State Phys. 372 (2008) 4505–4509, http://dx.doi.org/10.1016/j.physleta.2008.04.013.
[32] H. Chen, J. Ding, W. Guo, G. Chen, S. Ma, Blue-green emission mechanism and spectral shift of Al-doped ZnO films related to defect levels, RSC Adv. 3 (2013) 12327, http://dx.doi.org/10.1039/c3ra40750k.
[33] P.S. Xu, Y.M. Sun, C.S. Shi, F.Q. Xu, H.B. Pan, The electronic structure and spectral properties of ZnO and its defects, Nucl. Instrum. Methods Phys. Res. Sect. B: Beam Interact. Mater. At. 199 (2003) 286–290, http://dx.doi.org/10.1016/S0168-583X(02)01425-8.
[34] A.B. Djurišić, W.C.H. Choy, V.A.L. Roy, Y.H. Leung, C.Y. Kwong, K.W. Cheah, T.K. G. Rao, W.K. Chan, H.F. Lui, C. Surya, Photoluminescence and electron paramagnetic resonance of ZnO tetrapod structures, Adv. Funct. Mater. 14 (2004) 856–864, http://dx.doi.org/10.1002/adfm.200305082.
[35] V. Kumar, H.C. Swart, O.M. Ntwaeaborwa, R.E. Kroon, J.J. Terblans, S.K.K. Shaat, a Yousif, M.M. Duvenhage, Origin of the red emission in zinc oxide nanophosphors, Mater. Lett. 101 (2013) 57–60, http://dx.doi.org/10.1016/j.matlet.2013.03.073.
[36] C.H. Ahn, Y.Y. Kim, D.C. Kim, S.K. Mohanta, H.K. Cho, A comparative analysis of deep level emission in ZnO layers deposited by various methods, J. Appl. Phys. 105 (2009) 1–6, http://dx.doi.org/10.1063/1.3054175.
[37] M. Gomi, N. Oohira, K. Ozaki, M. Koyano, Photoluminescent and structural properties of precipitated ZnO fine particles, Jpn. J. Appl. Phys. 42 (2003) 481–485, http://dx.doi.org/10.1143/JJAP.42.481.
[38] V. Ney, S. Ye, T. Kammermeier, a Ney, H. Zhou, J. Fallert, H. Kalt, F.Y. Lo, a Melnikov, a D. Wieck, Structural, magnetic, and optical properties of Co- and Gd-implanted ZnO(0001) substrates, J. Appl. Phys. (2008), http://dx.doi.org/10.1063/1.3000452.